projected increases in heatwave events over Ireland (2021–2050), with a slight north-west to south-east gradient evident over the country. These results are consistent with the findings of the current report.

3.4 Frost and Ice Days

The large projected decrease in cold nights (Figure 3.6b; TMIN-5%) implies a decrease in the number of frost and ice days by the middle of the century. This is confirmed by Figure 3.8a and b, which present the projected annual change in the number of frost and ice days, respectively. Averaged over the whole country, the number of frost days (days when the minimum temperature is < 0°C) is projected to decrease by 45% and 58% for the RCP4.5 and RCP8.5 scenario, respectively. Similarly, the number of ice days (days when the maximum temperature is < 0°C) is projected to decrease by 68% and 78% for the RCP4.5 and RCP8.5 scenarios, respectively. For comparison, the observed annual mean numbers of frost and ice days for 1981–2000 are presented in Figure 3.9a and b, respectively (data from Walsh, 2012). Note that the observed number of ice days is small, particularly in coastal regions. It is worth noting that periods of frost and ice are important environmental drivers that trigger phenological phases in many plant and animal species. Changes in the occurrence of these weather types may disrupt the life cycles of these species (e.g. Williams *et al*., 2015; Bigler and Bugmann, 2018).

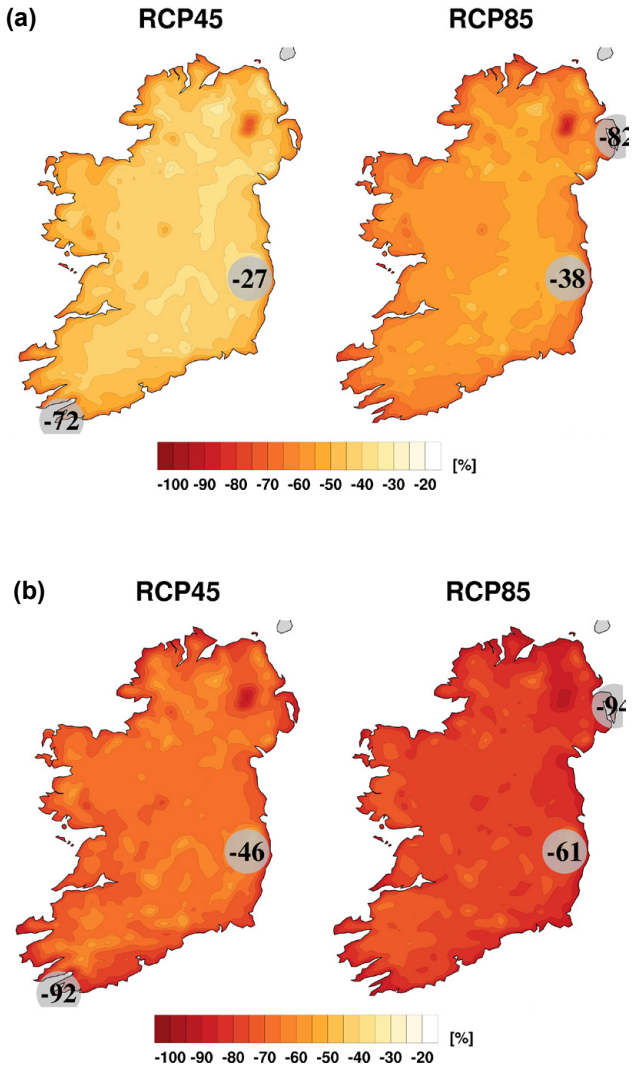

Figure 3.8. Projected changes in mid-century numbers of (a) frost days and (b) ice days. In each case, the future period, 2041–2060, is compared with the past period, 1981–2000. The numbers included on each plot are the minimum and maximum projected changes, displayed at their locations.

3.5 The Growing Season

Within a period of 12 months, the thermal growing season length is officially defined as the number of days between the first occurrence of at least 6 consecutive days with a daily mean temperature > 5°C and the first occurrence of at least 6 consecutive days with a daily mean temperature < 5°C.
Figure 3.10a shows a large projected increase in the average length of the growing season over Ireland by the middle of the century. There exists a clear south-to-north gradient, with values ranging from 5% to 18% and from 6% to 23% for the RCP4.5 and RCP8.5 scenarios, respectively. Averaged over the whole country, the length of the growing season is projected to increase by 12% and 16% for the RCP4.5 and RCP8.5 scenarios, respectively. Figure 3.10b, the projected change in the start of the growing season, shows that by the middle of the century the growing season is expected to start 10–31 days earlier for the RCP4.5 scenario and 10–36 days early for the RCP8.5 scenario. Averaged over the whole country, the growing season is projected to start 15 and 24 days early for the RCP4.5 and RCP8.5 scenarios, respectively.

For comparison, the observed length and start of the growing season over the period 1981–2000 (derived from daily mean temperature data provided by Walsh, 2012) are presented in Figure 3.11a and b, respectively.

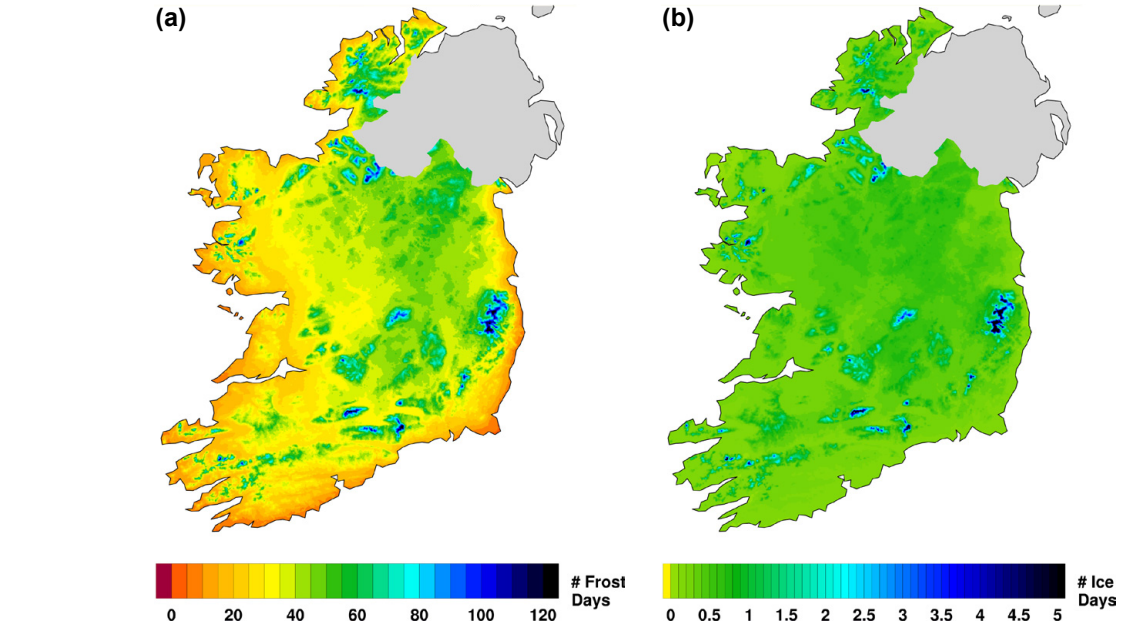

Figure 3.9. The observed mean annual number of (a) frost days and (b) ice days for the period 1981–2000.

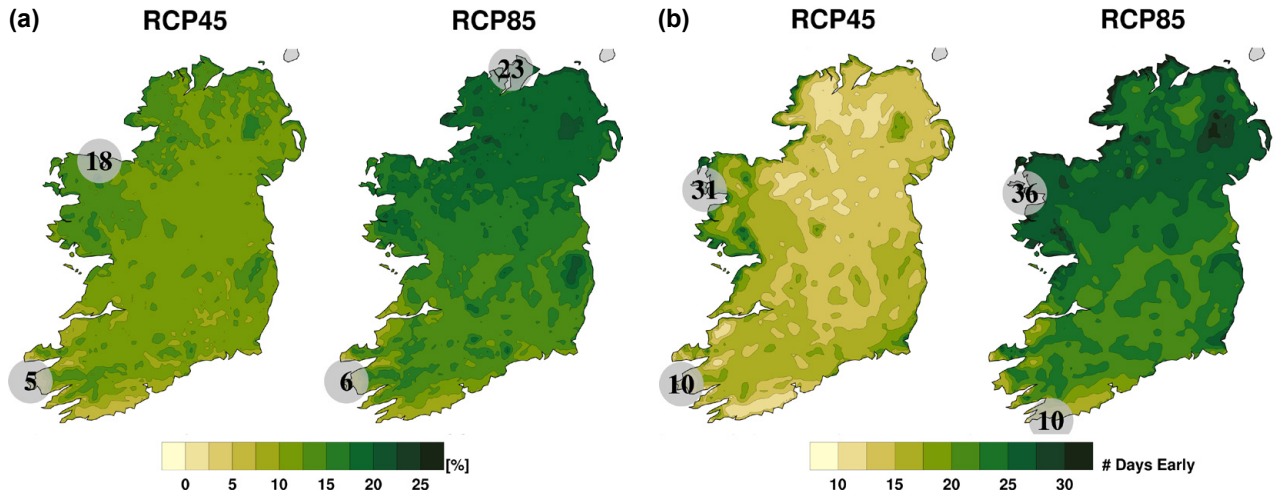

Figure 3.10. Mid-century projected changes in (a) the length of the growing season (%) and (b) the start of the growing season (number of days early). In each case, the future period, 2041–2060, is compared with the past period, 1981–2000. The numbers included on each plot are the minimum and maximum projected changes, displayed at their locations.

3.6 The Grazing Season

The growing season calculation is based solely on temperature and does not take into account the delay before sufficient plant cover is available to support grazing animals or the ability of animals and machinery to pass over land. The approximate length of the grazing season, in days per year, can be approximated from the following equation (Smith, 1976; Collins and Cummins, 1996):

$$GzS = 29.3T - 0.1R + 19.5 \quad (3.1)$$

where T is the mean annual 2-m temperature (°C) and R is the mean annual rainfall (mm year^{-1}).

Figure 3.12a shows that, by the middle of the century, the grazing season is projected to increase by 12–46 and 17–55 days per year for the RCP4.5 and RCP8.5 scenarios, respectively. Averaged over the whole country, the grazing season is projected to increase by

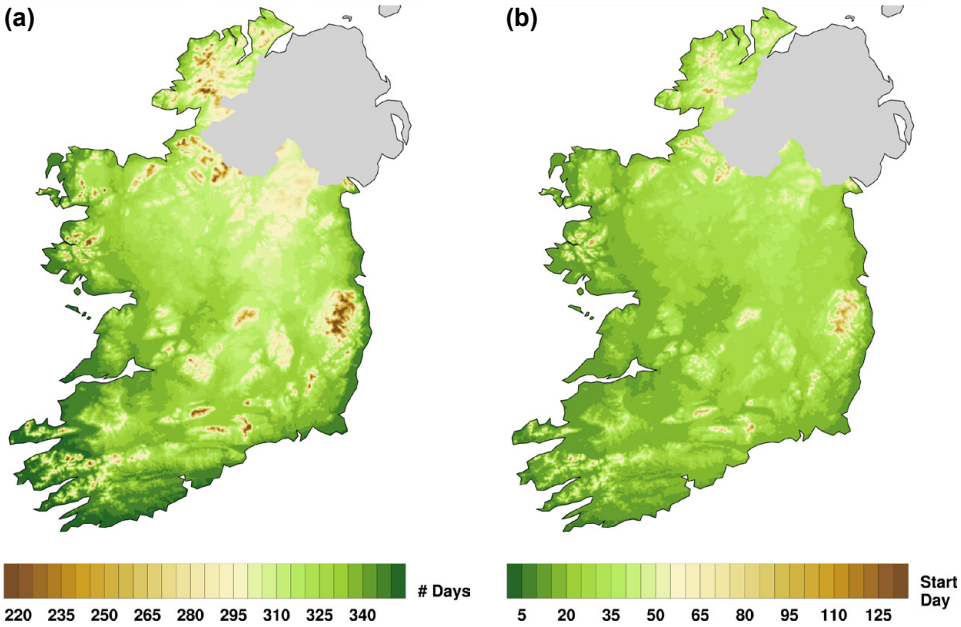

Figure 3.11. Observed growing season statistics for the period 1981–2000: (a) mean annual length and (b) mean start day of growing season (where day 1 is 1 January, day 2 is 2 January, etc.).

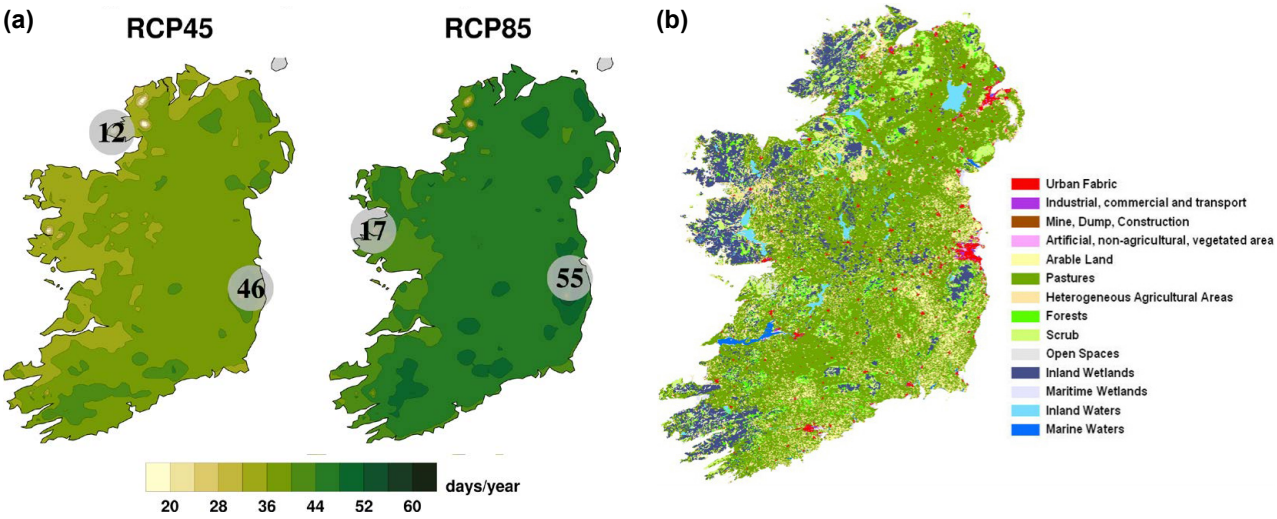

Figure 3.12. (a) Mid-century projected changes in the length of the grazing season and (b) the Coordination of Information on the Environment (Corine) land cover map of Ireland. The colours represent the land cover in 2006. Image reproduced with permission from Dwyer (2013).

37 and 45 days per year for the RCP4.5 and RCP8.5 scenarios, respectively.

It should be noted that not all areas presented in Figures 3.10 and 3.12a are suitable for agriculture and/or forestry. The projections should therefore be considered in the context of an observed soil/grass map, as presented in Figure 3.12b.

3.7 Growing Degree Days (Crops and Pests)

A degree day, an estimate of accumulated heat, is defined as the deviation (°C) from a reference temperature value (Fraisse *et al*., 2010; Project Team ECA&D, 2013; Kendon *et al*., 2015). Degree days represent the number of degrees by which the temperature has gone above or below a threshold.

Growing degree days (GDDs) are used to predict the growth and development of plants, insects and diseases of which the developments are very dependent on temperature and the daily accumulation of heat. The amount of heat required to advance a plant or pest to the next development stage remains constant from year to year; however, the actual amount of time (days) can vary considerably because of weather conditions. Each crop, insect and disease species has a minimum base temperature (T_b) or threshold below which development does not occur (Fraisse *et al*., 2010; OMAFRA, 2017). For example, in Europe, 5.5°C applies to wheat, barley, rye, oats and lettuce, 8°C to sunflowers and potatoes and 10°C to American maize, rice, corn, and tomato (McMaster and Wilhelm, 1997; Miller *et al*., 2001; Spinoni *et al*., 2015). See Table 3.1 for a list of base temperatures for crops and pests (McMaster and Wilhelm, 1997; Johnson *et al*., 1998; Miller *et al*., 2001; Spinoni *et al*., 2015).

The GDD was computed using the daily mean temperature (T_M) for different base temperatures (T_b), as described in Spinoni *et al*. (2015) and Project Team ECA&D (2013):

$$GDD_{daily} = \max\{(T_M - T_b), 0\} \quad (3.2)$$

$$GDD = \sum GDD_{daily} \quad (3.3)$$

Figure 3.13 shows that the GDDs for "crop base temperatures" 5.5°C, 8°C and 10°C are projected to increase substantially by the middle of the century. The projected increases are largest for the higher baseline temperatures. Averaged over the whole country, GDDs are projected to increase by 23% for RCP4.5 and 30% for RCP8.5 (T_b = 5.5°C); 32% for RCP4.5 and 42% for RCP8.5 (T_b = 8°C); and 45% for RCP4.5 and 59% for RCP8.5 (T_b = 10°C) (see Table 3.1). The results suggest a warming climate may present some positive opportunities for farming. However, the results should be viewed in the context that a warming climate will also result in an increase in pests as a result of an increase in heating and a decrease in frost and ice days (see section 3.4). Figure 3.14 and Table 3.1 show that the GDDs for "pest base temperatures" 6°C, 7°C, 9°C and 10°C are similarly projected to increase substantially by the middle of the century. Furthermore, projected increases in extreme temperatures (section 3.2), heatwaves (section 3.3), heavy precipitation (section 3.10) and dry periods/ droughts (section 3.11) will have substantial adverse effects on agriculture in Ireland by the middle of the century.

3.8 Ontario Crop Heat Units

The Ontario Crop Heat Unit (OCHU) is a variant of a degree day accumulation and is widely used to rate the suitability of regions for production of corn/ maize (Collins and Cummins, 1996; Bootsma *et al*., 1999, 2007; OMAFRA, 2017). The OCHU model uses separate calculations for maximum and minimum temperatures. The maximum or daytime relationship (Y_{max}) uses 10°C as the base temperature and has a curvilinear response to temperature with a maximum

Table 3.1. Growing degree days base temperature for various crops and pests, and mid-century projected change averaged over all land points of Ireland

	Base temperature (°C)	Projection (all Ireland)	
		RCP4.5 (%)	RCP8.5 (%)
Crops			
Wheat, barley, rye, oats and lettuce	5.5	+23	+30
Sunflower, potato	8	+32	+42
American maize, rice, corn and tomato	10	+45	+59
Pests			
Stalk borer	6	+25	+32
Corn rootworm[a]	7	+28	+36
Lucerne weevil	9	+38	+49
Black cutworm, European corn borer and standard baseline for insect and mite pests of woody plants	10	+45	+59

[a]**Reported in the UK but currently not present in Ireland.**

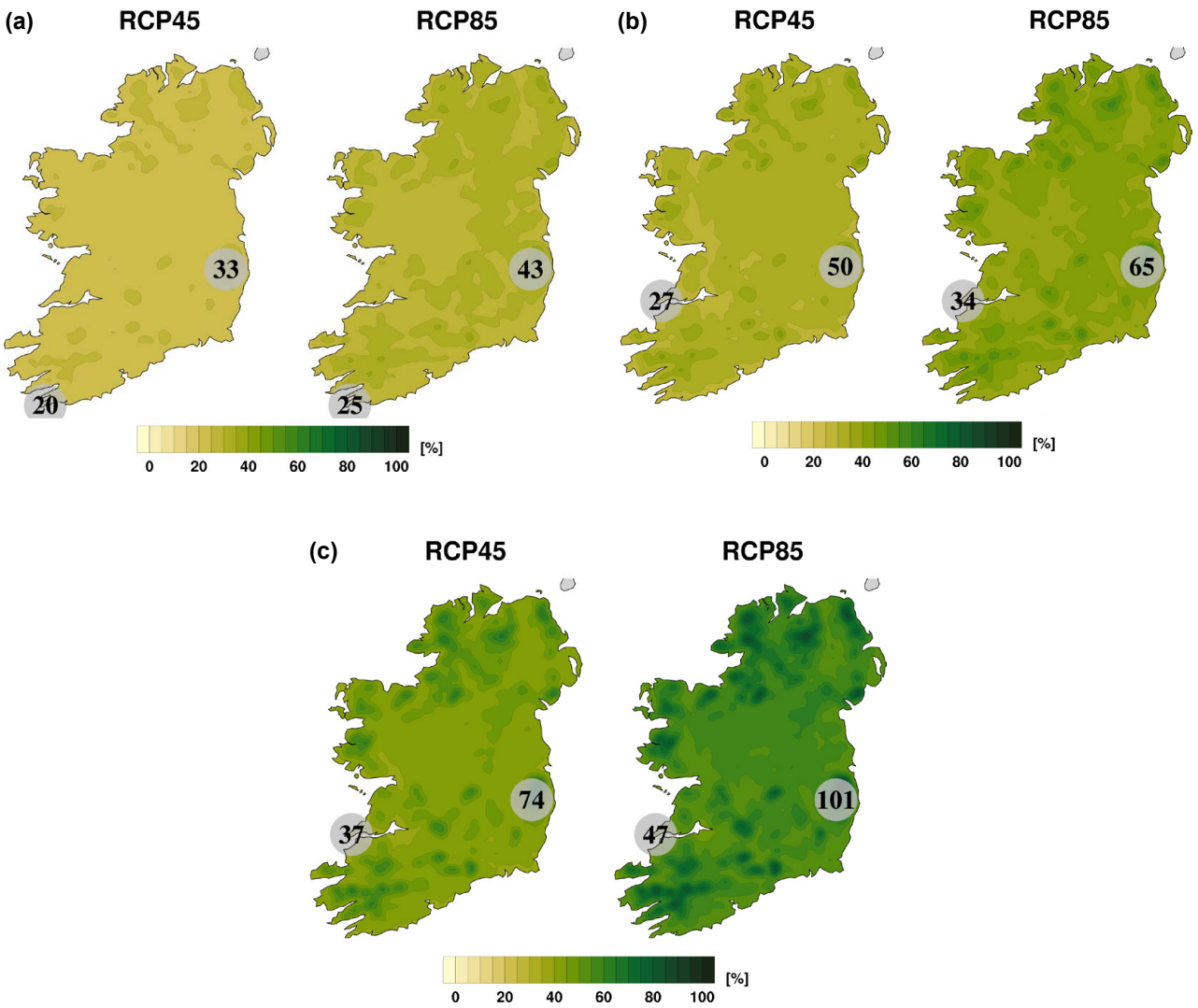

Figure 3.13. Mid-century projected changes (%) in GDDs for "crop base temperatures": (a) T_b = 5.5°C (wheat, barley, rye, oats and lettuce), (b) T_b = 8°C (sunflower and potato) and (c) T_b = 10°C (American maize, rice, corn and tomato). In each case, the future period, 2041–2060, is compared with the past period, 1981–2000. The numbers included on each plot are the minimum and maximum projected changes, displayed at their locations.

at 30°C; no growth occurs below 10°C and growth peaks at 30°C and declines thereafter. The minimum (or night-time) relationship uses 4.4°C as the base temperature, with the response above this being linear; Y_{min} does not specify an optimum temperature because night-time minimum temperatures very seldom exceed 25°C. Mean annual OCHU values for May to September are calculated using daily values as follows:

$$\text{Daily OCHU} = \frac{Y_{max} + Y_{min}}{2} \quad (3.4)$$

where

$$Y_{max} = \max\{3.33(T_{max} - 10) - 0.084(T_{max} - 10)^2, 0\}, \quad (3.5)$$

$$Y_{min} = \max\{1.8(T_{min} - 4.44), 0\} \quad (3.6)$$

and T_{min} and T_{max} are the daily minimum and maximum temperatures, respectively.

Figure 3.15 shows that, by the middle of the century, OCHUs (May to September) are projected to increase by 18–38% and 23–49% for the RCP4.5 and RCP8.5 scenarios, respectively. Averaged over the whole country, OCHUs are projected to increase by 23% and 29% for the RCP4.5 and RCP8.5 scenarios, respectively.

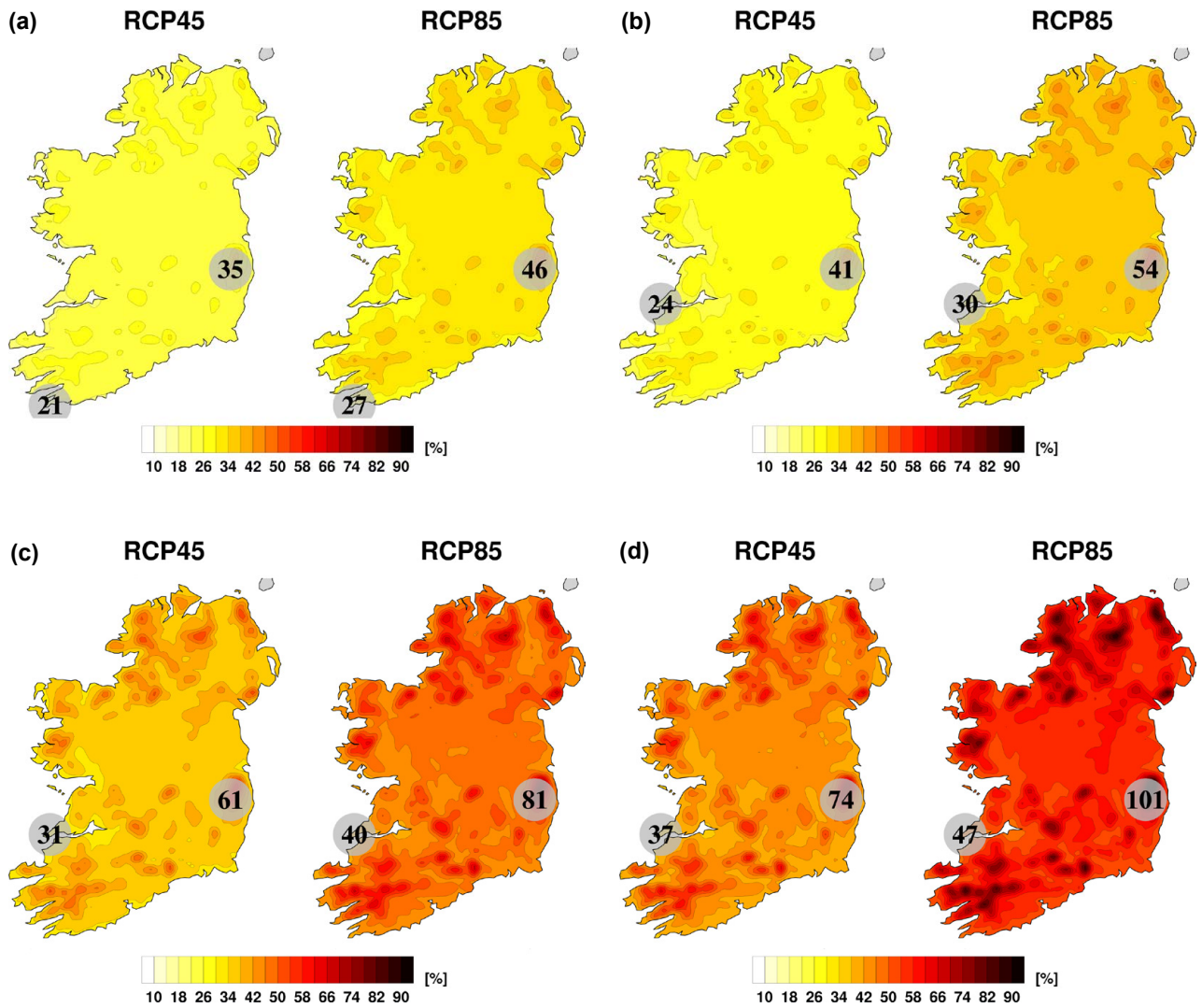

Figure 3.14. Mid-century projected changes (%) in GDDs for "pest base temperatures": (a) T_b = 6°C (stalk borer), (b) T_b = 7°C (corn rootworm), (c) T_b = 9°C (Lucerne weevil) and (d) T_b = 10°C (black cutworm, European corn borer and standard baseline for insect and mite pests of woody plants). In each case, the future period, 2041–2060, is compared with the past period, 1981–2000. The numbers included on each plot are the minimum and maximum projected changes, displayed at their locations.

3.9 Mid-century Precipitation Projections

Figure 3.16 presents the mean annual percentage change in precipitation for the RCP4.5 and RCP8.5 scenarios. There is an indication of a slight reduction in the annual precipitation of ≈0–6% for the RCP4.5 scenario. However, projected reductions are small (≈0%) over most of the country for both scenarios.

Figure 3.17a presents the seasonal change (%) in precipitation for the RCP4.5 scenario; the corresponding plots for RCP8.5 are presented in Figure 3.17b. The strongest signals are a projected decrease for summer, with the largest impacts for the RCP8.5 scenario. The summer reductions range from ≈0% to 11% for the RCP4.5 scenario and from 2% to 17% for the RCP8.5 scenario. Other seasons show a small projected change in precipitation, with the exception of winter under the RCP8.5 scenario, where precipitation is expected to increase by ≈0 to 11%.

The projected precipitation changes of the current study vary greatly between ensemble members, much more so than for the temperature projections (see section 3.1). The regional details of Figures 3.16 and 3.17 are therefore not reliable. Furthermore, the disagreement between RCM projections can result in large individual outliers skewing the mean ensemble

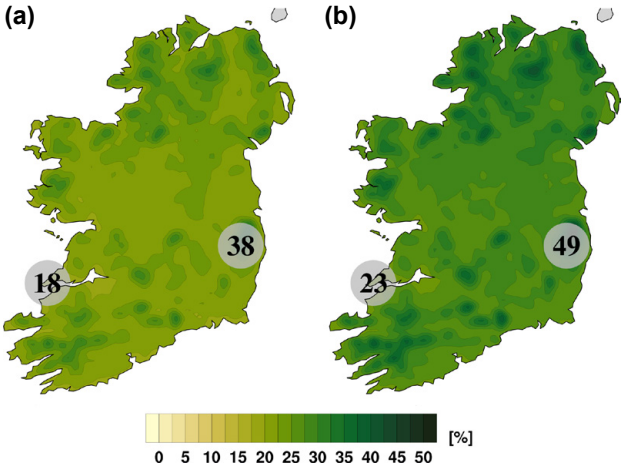

Figure 3.15. Mid-century projected changes (%) in OCHUs during May to September for the (a) RCP4.5 and (b) RCP8.5 scenarios. In each case, the future period, 2041–2060, is compared with the past period, 1981–2000. The numbers included on each plot are the minimum and maximum projected changes, displayed at their locations.

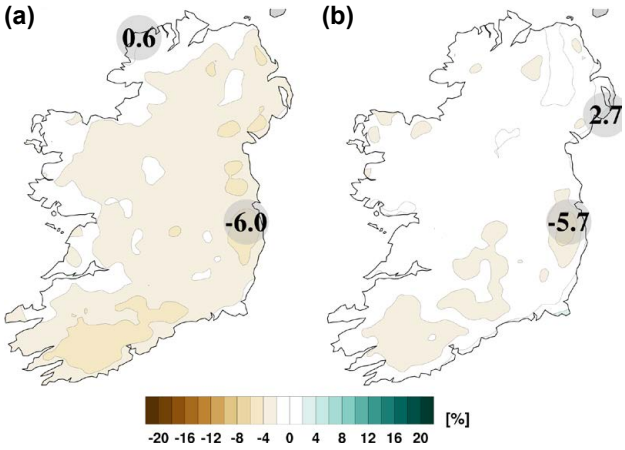

Figure 3.16. Ensemble mean of mid-century annual precipitation projections (%) for the (a) RCP4.5 and (b) RCP8.5 scenarios. In each case, the future period, 2041–2060, is compared with the past period, 1981–2000. The numbers included on each plot are the minimum and maximum projected changes, displayed at their locations.

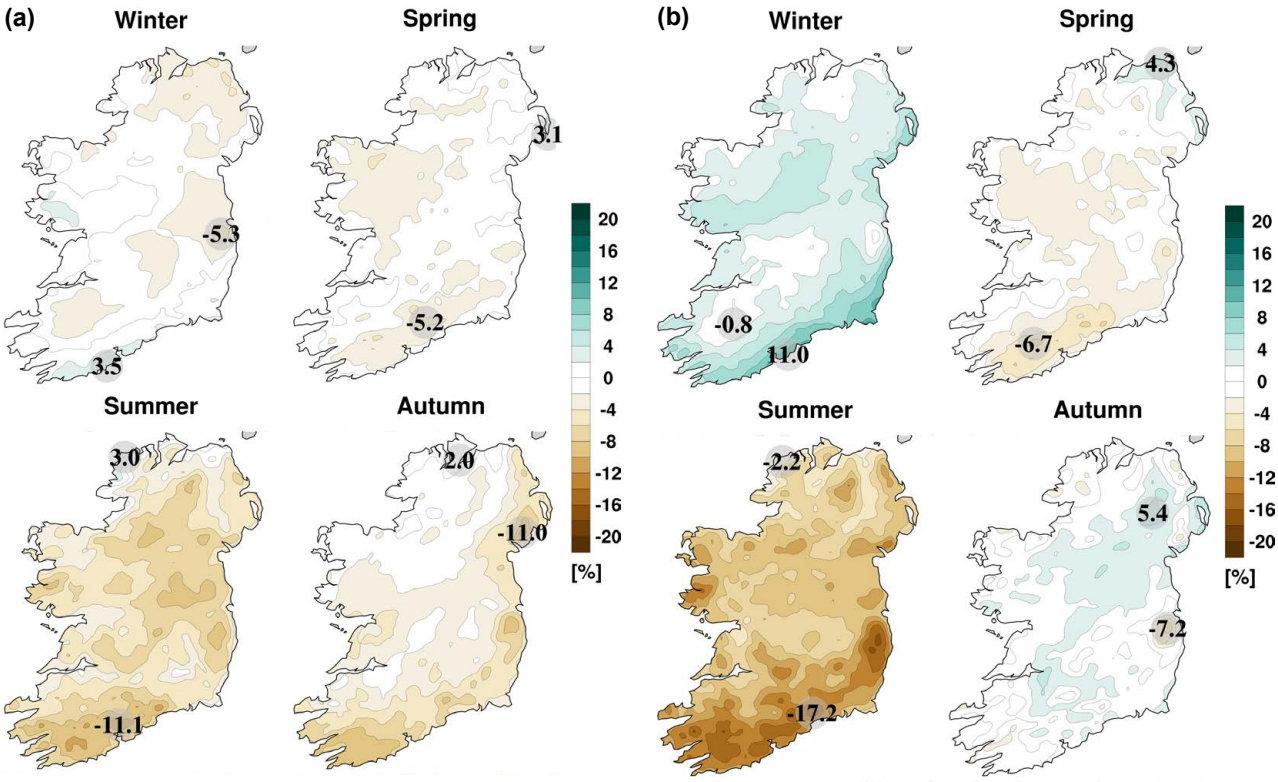

Figure 3.17. Mid-century seasonal projections of mean precipitation (%) for the (a) RCP4.5 and (b) RCP8.5 scenarios. In each case, the future period, 2041–2060, is compared with the past period, 1981–2000. The numbers included on each plot are the minimum and maximum projected changes, displayed at their locations.

projection. It is therefore more informative to consider the 33rd, 50th and 66th percentile projections as presented in Figure 3.18. The likelihood values are calculated at each grid point using the full RCM ensemble of projections, as outlined in Table 1.2. The figures show that there is large uncertainty in the projections, as demonstrated by a disagreement between the percentile projections. The exceptions

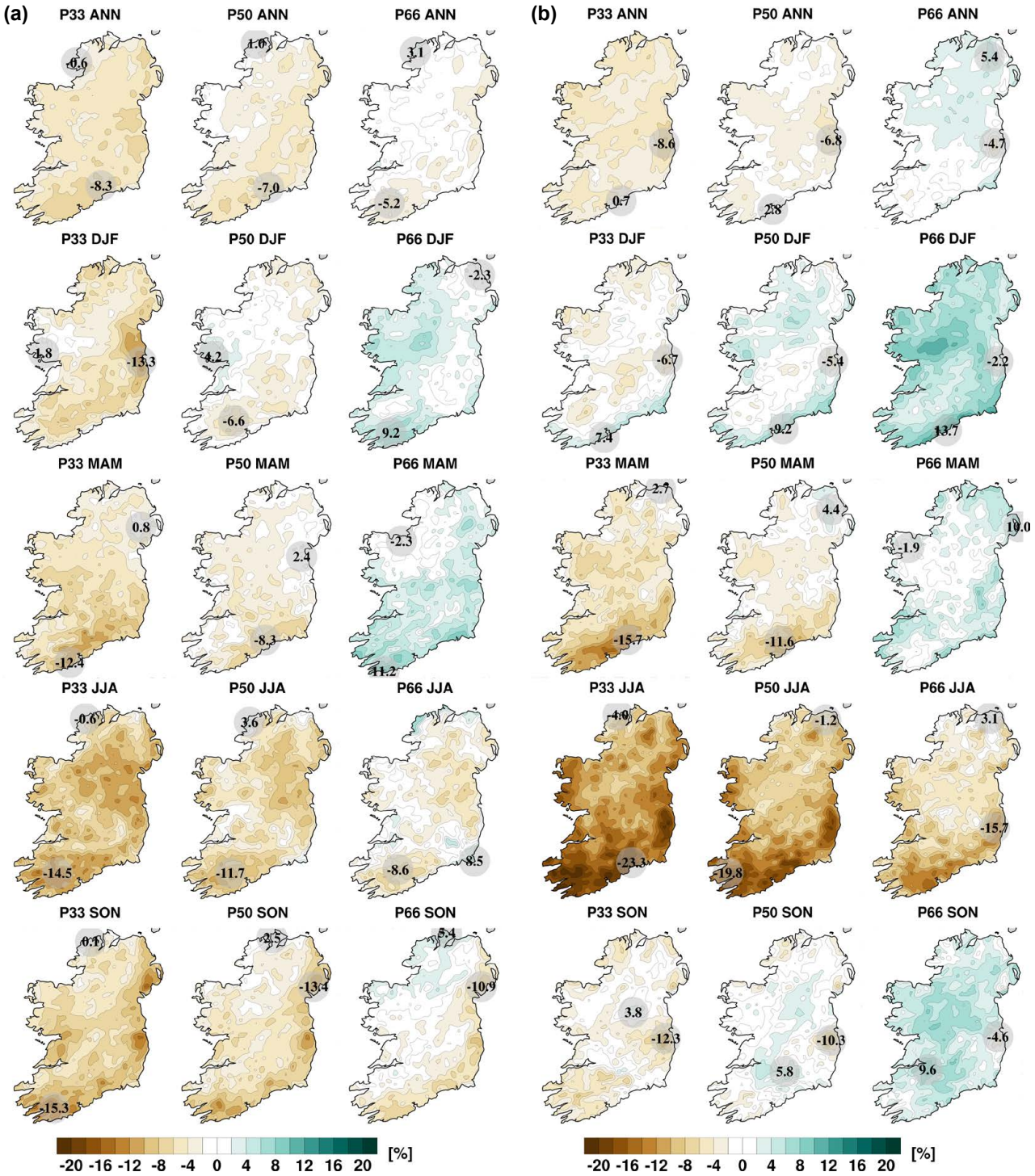

Figure 3.18. The 33rd, 50th and 66th percentiles of annual and seasonal mean precipitation projections (%) for the (a) RCP4.5 and (b) RCP8.5 scenarios. In each case, the future period, 2041–2060, is compared with the past period, 1981–2000. The numbers included on each plot are the minimum and maximum projected changes, displayed at their locations. ANN, annual; DJF, December, January, February; JJA, June, July, August; MAM, March, April, May; SON, September, October, November.

are summer (both RCP4.5 and RCP8.5 scenarios) and annual and autumn (RCP4.5 projections), when the signals are more robust. The strongest signal is for a substantial drying during summer, when there is a clear agreement between the percentiles (for both the RCP4.5 and RCP8.5 scenarios).

3.9.1 Changes in the variability of the precipitation climate

The uncertainty of the mean precipitation projections may be partly attributed to a projected increase in the variability of the future Irish precipitation climate, resulting in an increase in both dry periods and heavy rainfall events. This is clearly demonstrated in Figures 3.19 and 3.20, which present the annual and seasonal projected change in the standard deviation of 3-hour precipitation, respectively. It is noted that the standard deviation of precipitation is expected to increase substantially for all seasons by the middle of the century, with the exception of spring, when the signal is less pronounced for the RCP8.5 scenario.

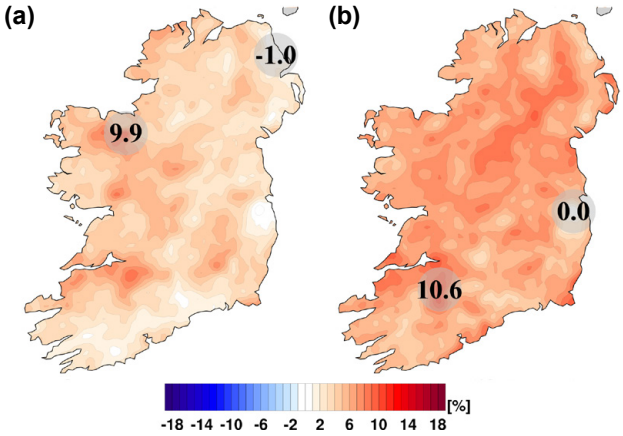

Figure 3.19. Annual projected change in the standard deviation of precipitation (%) for the (a) RCP4.5 and (b) RCP8.5 scenarios. In each case, the future period, 2041–2060, is compared with the past period, 1981–2000. The numbers included on each plot are the minimum and maximum projected changes, displayed at their locations.

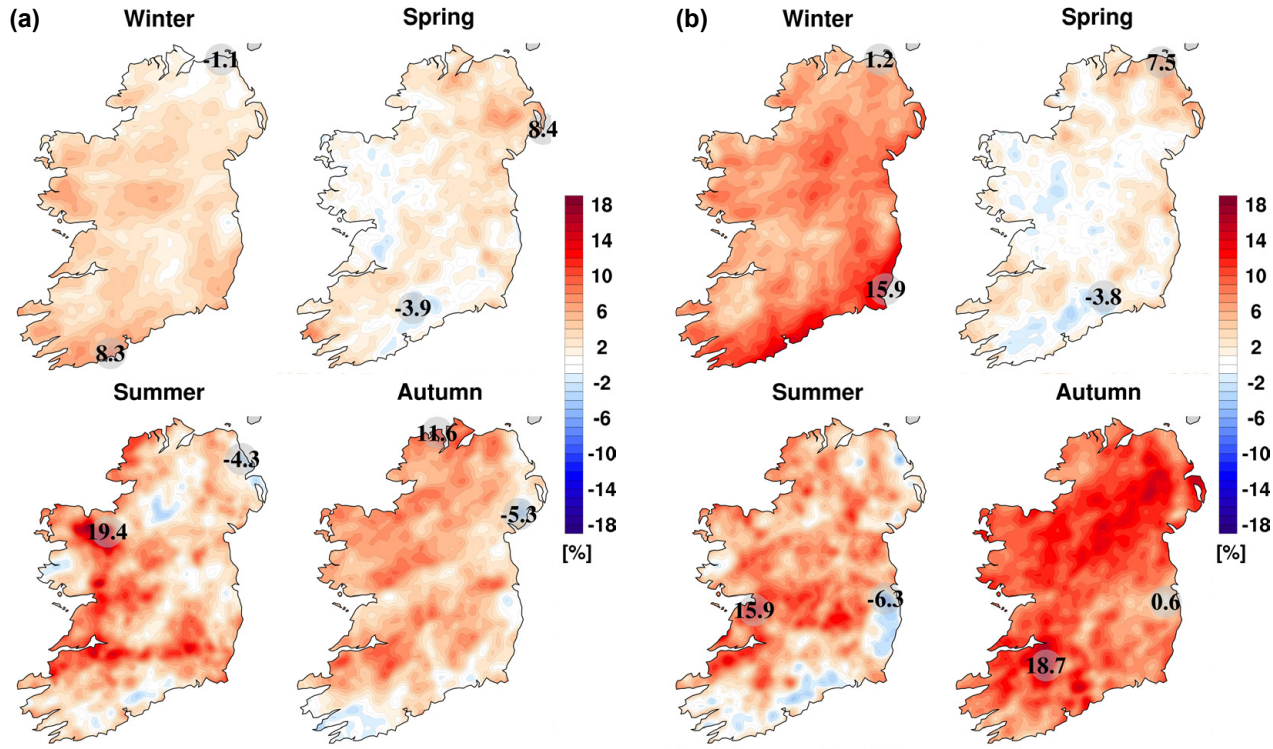

Figure 3.20. Seasonal projected change in the standard deviation of precipitation (%) for the (a) RCP4.5 and (b) RCP8.5 scenarios. In each case, the future period, 2041–2060, is compared with the past period, 1981–2000. The numbers included on each plot are the minimum and maximum projected changes, displayed at their locations.

The large projected change in the standard deviation of precipitation, coupled with small changes in the mean, imply an increase in both dry periods and heavy rainfall events (i.e. the tails of rainfall distribution will become more pronounced; see Figure 1.3b for a schematic example of such an outcome). This is confirmed by Figures 3.21 and 3.22, which show large projected changes in intense rainfall events and dry periods, respectively. The projections of increased variability of the precipitation climate will have adverse implications for society (e.g. droughts, flooding, water management and housing) and sectors of the economy, such as agriculture. Furthermore, the increase in frequency of both droughts and heavy rainfall events could be detrimental to potential gains of a warming climate to the agricultural sector, as discussed in sections 3.5–3.8.

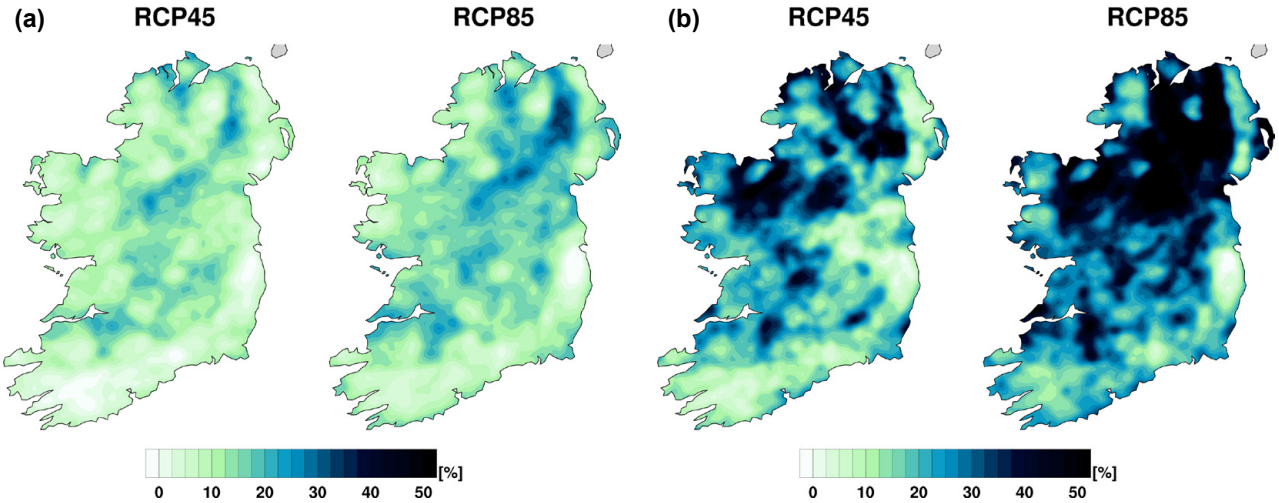

Figure 3.21. Projected changes (%) in mid-century number of annual (a) wet days (precipitation > 20 mm day^{-1}) and (b) very wet days (precipitation > 30 mm day^{-1}). In each case, the future period, 2041–2060, is compared with the past period, 1981–2000.

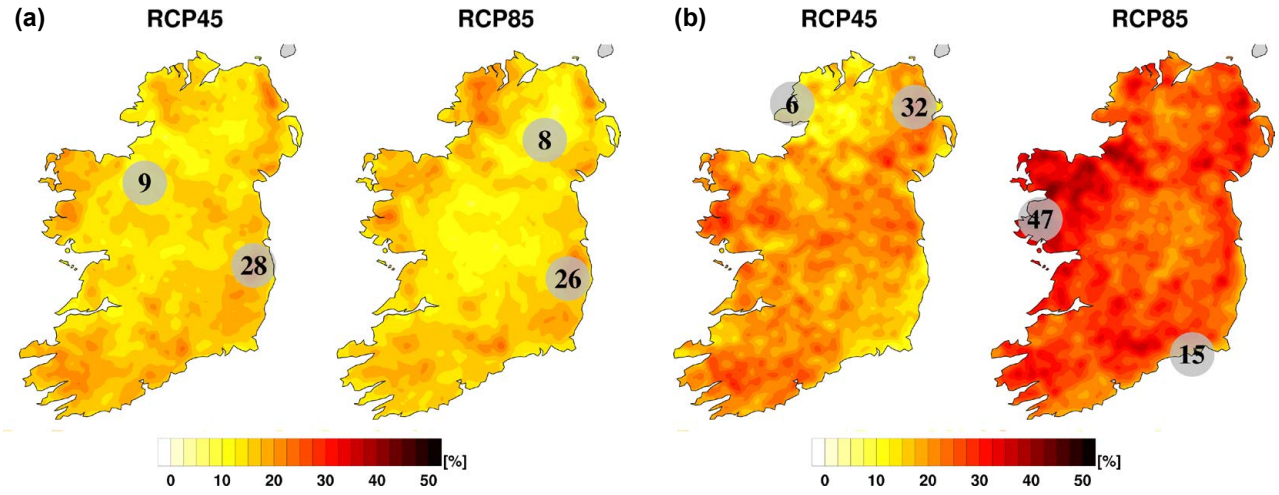

Figure 3.22. Projected changes (%) in mid-century number of dry periods (a) annually and (b) in summer. In each case, the future period, 2041–2060, is compared with the past period, 1981–2000. The numbers included on each plot are the minimum and maximum projected changes, displayed at their locations.

3.10 Heavy Precipitation Events

Changes in the occurrence of heavy rainfall events are of particular importance because of the link with flooding. In this section, mid-century projections of "wet days" and "very wet days" are presented. A "wet day" is defined as one on which the daily precipitation amount is greater than 20 mm. A "very wet day" is defined as one on which the daily precipitation is greater than 30 mm.[10] Figure 3.21a indicates an increase in the annual number of wet days for the RCP4.5 (mean value 10%) and RCP8.5 (mean value 14%) scenarios. The largest increases in wet days are expected for the autumn (9% for RCP4.5; 16% for RCP8.5) and winter (17% for RCP4.5; 26% for RCP8.5) months; a small increase is projected for summer (≈10% for both scenarios) and a mixed signal was found for spring. The projected increase in the annual number of very wet days, presented in Figure 3.21b, is substantial, with mean values of 21% and 31% for the RCP4.5 and RCP8.5 scenarios, respectively. Again, the largest increases were noted for the autumn (25% for RCP4.5; 42% for RCP8.5) and winter (33% for RCP4.5; 61% for RCP8.5) months.

A "likely" increase was also noted in the number of annual wet days (5% for RCP4.5; 8% for RCP8.5), annual very wet days (8% for RCP4.5; 19% for RCP8.5), autumn wet days (1% for RPC4.5; 6% for RCP8.5), autumn very wet days (3% for RCP4.5; 18% for RCP8.5), winter wet days (4% for RCP4.5; 12% for RCP8.5) and winter very wet days (2% for RCP4.5; 18% for RCP8.5).[11] It follows that it is "likely" that increases in heavy rainfall events will be greater than or equal to these values. The increased frequency of heavy precipitation is well marked in winter and autumn and over the full year, particularly for the RCP8.5 scenario, but regional details are not reliable because of a large spread in the ensembles. The projected increase in heavy rainfall events during autumn, winter and over the full year is consistent with the large projected change in standard deviation of the 3-hour precipitation presented in Figures 3.19 and 3.20.

The projected increase in the number of wet and very wet days should be considered in the context of historical values. Figure 3.23 presents the annual number of observed wet and very wet days, averaged

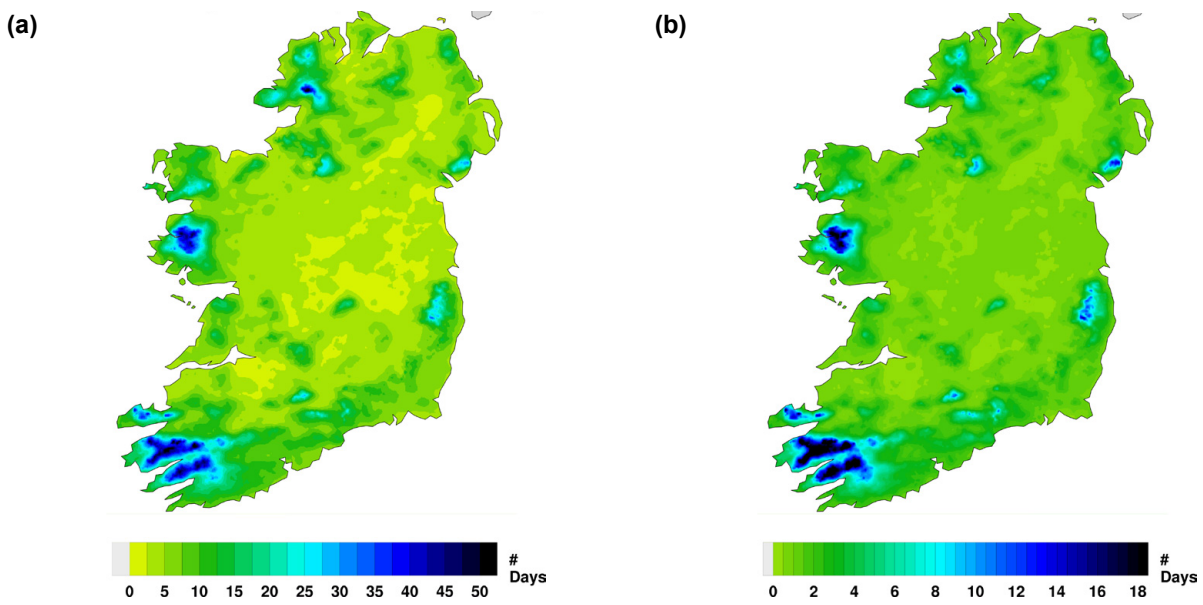

Figure 3.23. The observed number of mean annual (a) wet days (precipitation > 20 mm) and (b) very wet days (precipitation > 30 mm) averaged over the 20-year period 1981–2000. Note the different scales for each figure.

10 Note that these definitions apply only to the current study and were chosen to reflect amounts considered extreme in an Irish context. Such values would be considered less (more) extreme in wetter (dryer) regions of the planet.

11 Spatial figures are not presented for the "likely" projections of heavy precipitation events, as the regional details are highly variable and therefore not reliable. Current work focuses on reducing this regional uncertainty by increasing the RCM ensemble size and using more up-to-date RCMs to downscale CMIP6 global data.

over the 20-year period 1981–2000. Seasonal figures (not shown) present a similar geographical trend.

The projected change in heavy rainfall events are in line with previous RCM studies for Ireland, which showed large projected increases in intense rainfall by the middle of the century, particularly during the winter and autumn months (e.g. Gleeson *et al*., 2013; Nolan, 2015; Nolan *et al*., 2017).

3.11 Dry Periods

To quantify the potential impact of climate change on future drought events, the change in the number of dry periods was analysed. A dry period is defined as at least 5 consecutive days on which the daily precipitation is less than 1 mm.

Figure 3.22a indicates an increase in the annual number of dry periods for the RCP4.5 and RCP8.5 scenarios (mean value ≈16% for both RCPs). The largest increases in dry periods are expected for the summer months (20% for RCP4.5; 27% for RCP8.5 ; see Figure 3.22b). Substantial increases in dry periods are also expected for winter and autumn; projections are similar for both seasons, with an expected increase of ≈20% for both scenarios. A mixed signal was found for spring.

A "likely" increase was also noted in the number of annual (≈9% for both RCPs), winter (≈9% for both RCPs), summer (11% for RCP4.5; 18% for RCP8.5) and autumn (≈10% for both RCPs) dry periods. It follows that it is "likely" that increases in dry periods will be greater than or equal to these values. The projected increase in the frequency of dry periods is well marked in summer, winter, autumn and over the full year, but regional details are not reliable because of a large spread in the ensembles. The projected increase in dry periods during winter, summer, autumn and over the full year is consistent with the large projected change in standard deviation of precipitation (presented in Figures 3.19 and 3.20).

The projected percentage increase in the number of dry periods should be considered in the context of the historical number of dry periods. Figure 3.24 presents the observed number of dry periods annually and in autumn and summer, averaged over the 20-year period 1981–2000. The number of dry periods during winter (not shown) is similar to autumn. The projections of increased dry periods during summers are in line with observed precipitation trends. Murphy *et al*. (2017) analysed a continuous 305-year (1711–2016) monthly rainfall series and found statistically significant decreasing trends in summer rainfall.

The projected changes in dry periods are in line with previous RCM studies for Ireland, which showed large projected increases in dry events by the middle of the century, particularly during the summer and autumn months (e.g. Gleeson *et al*., 2013; Nolan, 2015; Nolan *et al*., 2017). The current study has additionally demonstrated a "likely" increase in dry periods during mid-century winter months.

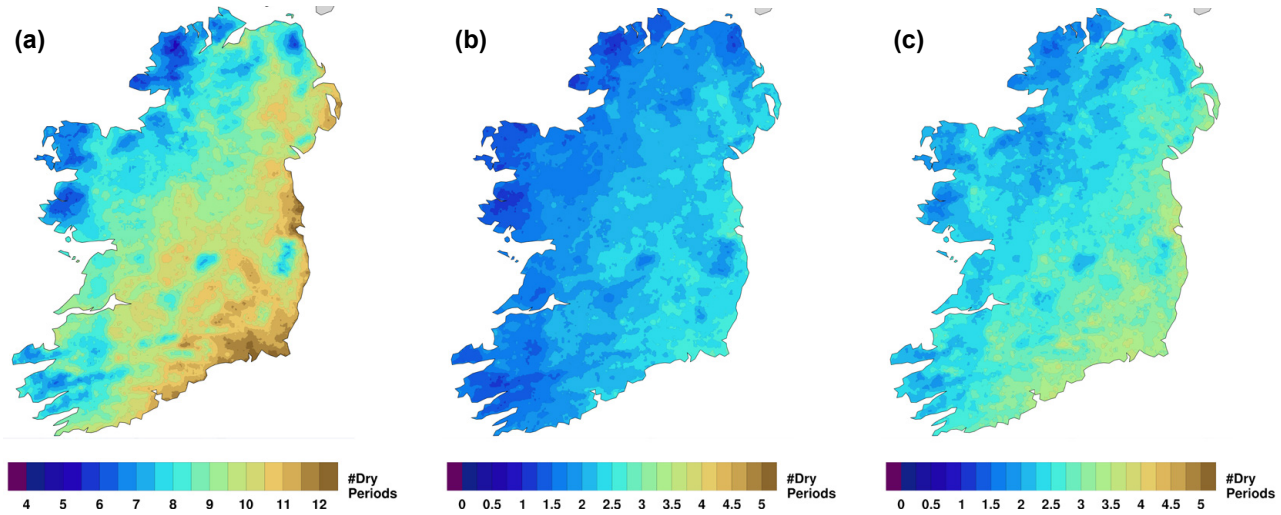

Figure 3.24. The observed number of dry periods averaged over the 20-year period 1981–2000 (a) annually, (b) in autumn and (c) in summer. Note the different scale for the annual figure.

3.12 Snowfall Projections

Figure 3.25 shows that annual snowfall is projected to decrease substantially by the middle of the century for the RCP4.5 (mean value 52%) and RCP8.5 scenarios (mean value 63%). The largest decreases are noted over low-lying regions. Figure 3.26 shows a small variation between the 33rd, 50th and 66th projection percentiles, which demonstrates good agreement (small spread) between ensemble members. Averaged over the whole country, the "likely" decreases in mid-century snowfall are 51% and 60% for the RCP4.5 and RCP8.5 scenarios, respectively.

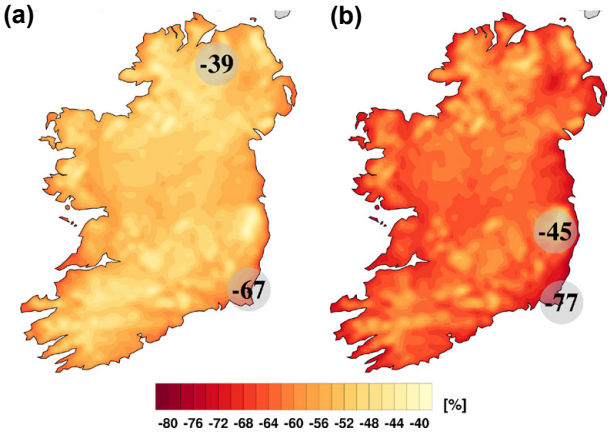

Figure 3.25. Ensemble mean of mid-century snowfall projections (%) for the (a) RCP4.5 and (b) RCP8.5 scenarios. In each case, the future period, 2041–2060, is compared with the past period, 1981–2000. The numbers included on each plot are the minimum and maximum projected changes, displayed at their locations.

3.13 10-m Wind Speed Projections

Figure 3.27 presents the mean annual percentage change in 10-m wind speed for the RCP4.5 and RCP8.5 scenarios. For the purpose of offshore wind energy and shipping applications, the analyses of wind speed cover all land points and a small portion

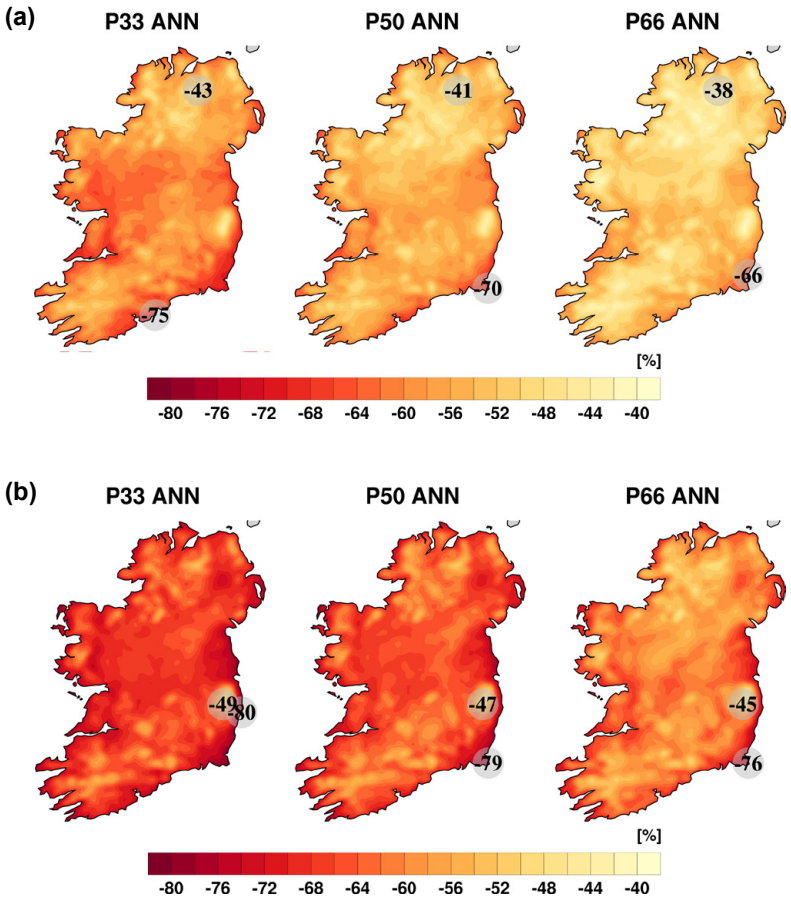

Figure 3.26. The 33rd, 50th and 66th percentiles of annual snowfall projections (%) for the (a) RCP4.5 and (b) RCP8.5 scenarios. In each case, the future period, 2041–2060, is compared with the past period, 1981–2000. The numbers included on each plot are the minimum and maximum projected changes, displayed at their locations.

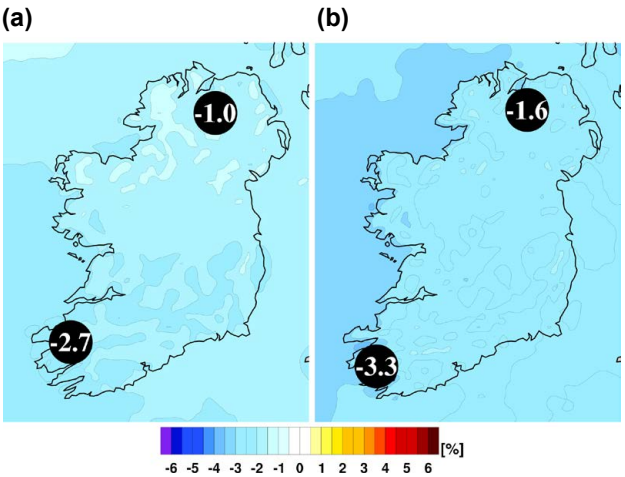

Figure 3.27. Ensemble mean of mid-century 10-m wind speed projections (%) for the (a) RCP4.5 and (b) RCP8.5 scenarios. In each case, the future period, 2041–2060, is compared with the past period, 1981–2000. The numbers included on each plot are the minimum and maximum projected changes over land, displayed at their locations.

of the surrounding sea. The projections show a slight reduction in the 10-m wind speed of 1–2.7% (mean value 1.8%) for the RCP4.5 scenario and 1.6–3.3% (mean value 2.6%) for the RCP8.5 scenario. Figure 3.28a presents the seasonal change (%) in 10-m wind speed for the RCP4.5 scenario; the corresponding plots for RCP8.5 are presented in Figure 3.28b. All seasons show a projected decrease in mean 10-m wind speed. The decreases are largest for summer under the RCP8.5 scenario. The summer reductions range from 0.3% to 3.4% for the RCP4.5 scenario and from 2% to 5.4% for the RCP8.5 scenario.

With the exception of spring and autumn under the RCP4.5 scenario, Figure 3.29 shows a small variation between the 33rd, 50th and 66th 10-m wind speed projection percentiles. This agreement adds a level of confidence to the projected reductions during summer (both RCPs), winter (both RCPs), spring (RCP8.5), autumn (RCP8.5) and over the full year (both RCPs).

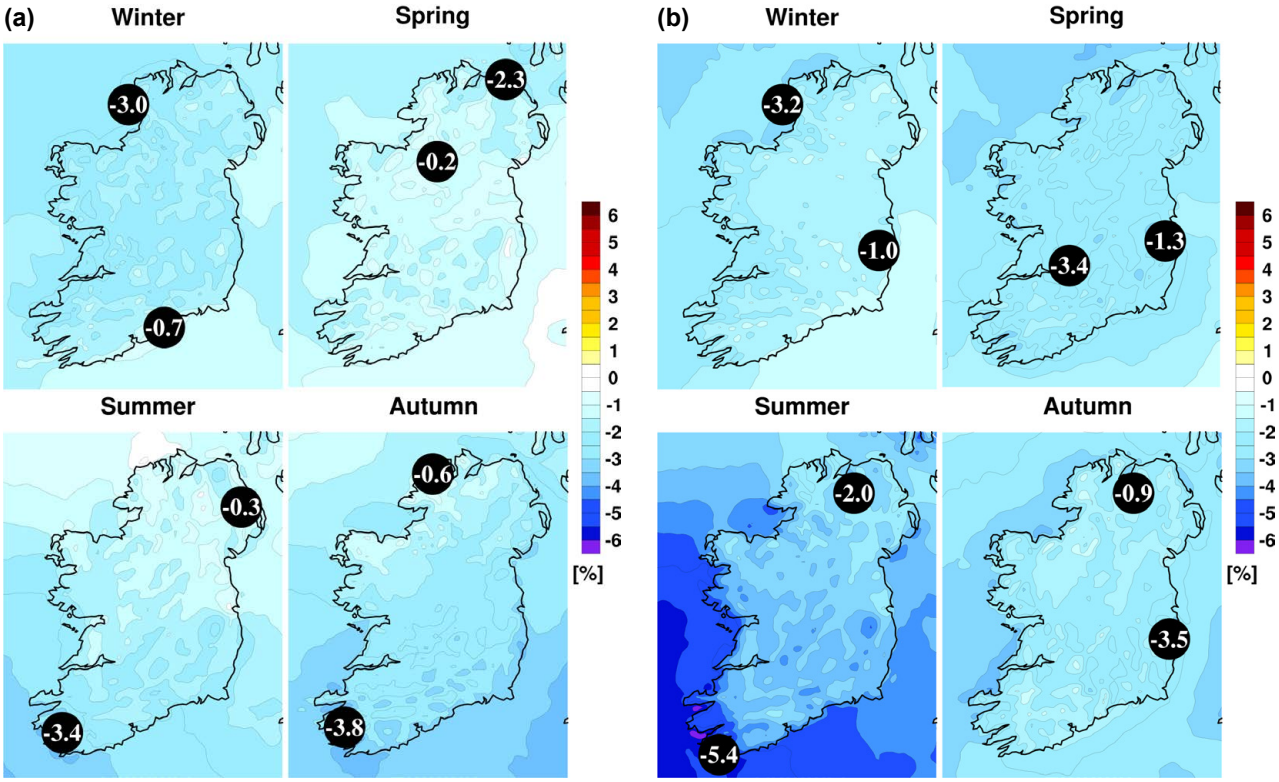

Figure 3.28. Mid-century seasonal projections of mean 10-m wind speed (%) for the (a) RCP4.5 and (b) RCP8.5 scenarios. In each case, the future period, 2041–2060, is compared with the past period, 1981–2000. The numbers included on each plot are the minimum and maximum projected changes, over land, displayed at their locations.

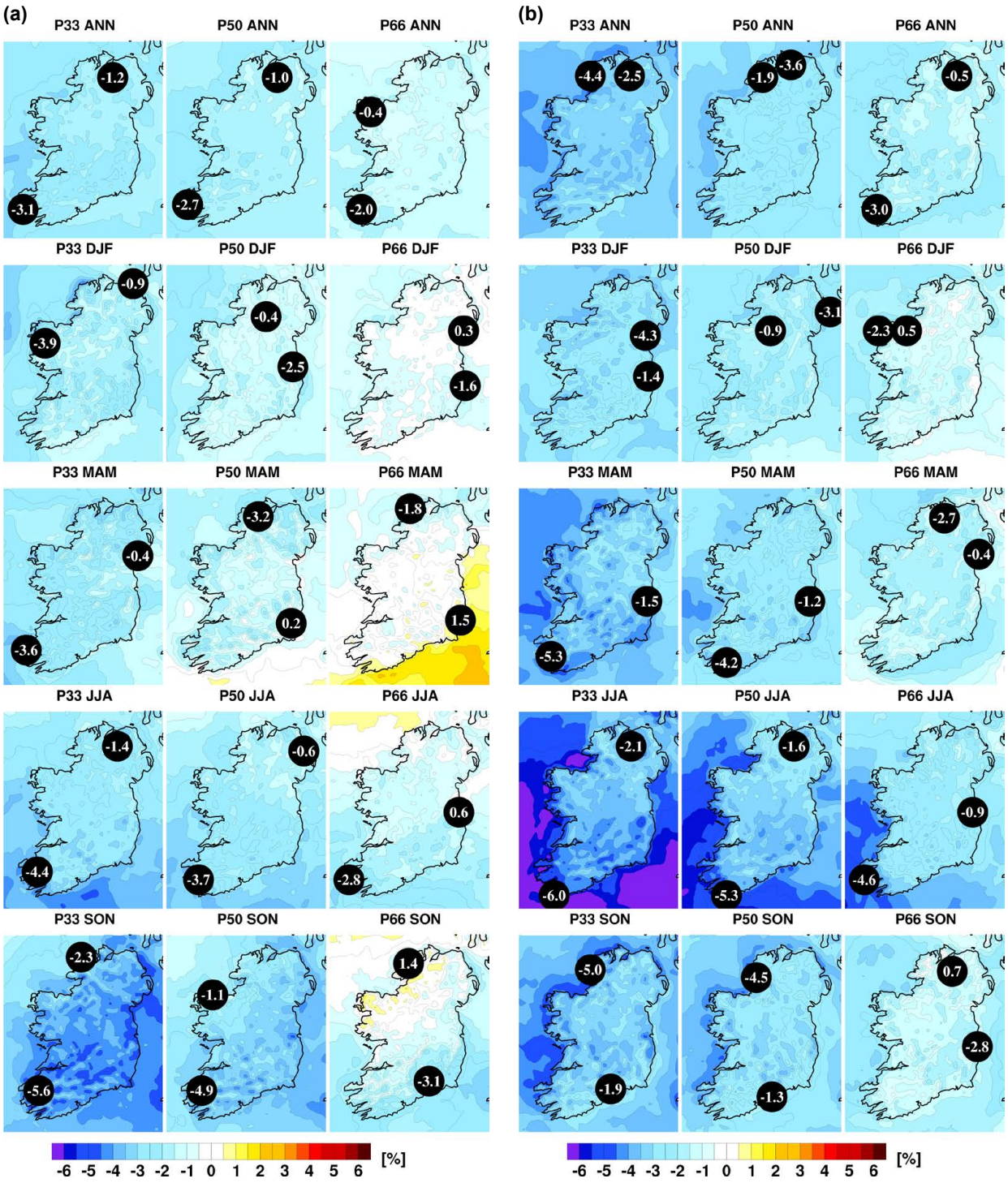

Figure 3.29. The 33rd, 50th and 66th percentiles of annual and seasonal mean 10-m wind speed projections (%) for the (a) RCP4.5 and (b) RCP8.5 scenarios. In each case, the future period, 2041–2060, is compared with the past period, 1981–2000. The numbers included on each plot are the minimum and maximum projected changes over land, displayed at their locations. ANN, annual; DJF, December, January, February; JJA, June, July, August; MAM, March, April, May; SON, September, October, November.

The annual change in the standard deviation of 10-m wind speed (Figure 3.30) shows small changes of ≈−2% to ≈0% for both the RCP4.5 and RCP8.5 scenarios. Similarly, the seasonal projected changes in the standard deviation of 10-m wind speed are small (Figure 3.31). All seasons – except winter, where small (≈0%) changes are noted – show reductions, with the largest decreases noted during summer. A reduction

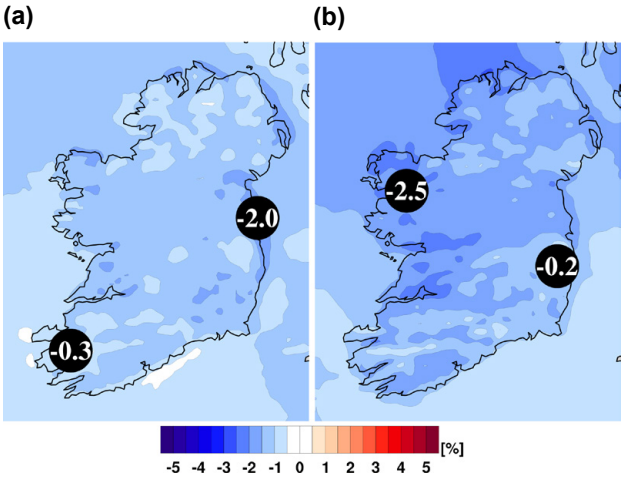

Figure 3.30. Annual projected change in the standard deviation of 10-m wind speed (%) for the (a) RCP4.5 and (b) RCP8.5 scenarios. In each case, the future period, 2041–2060, is compared with the past period, 1981–2000. The numbers included on each plot are the minimum and maximum projected changes, displayed at their locations.

in mean 10-m wind speed, coupled with a decrease in standard deviation, implies a shift to the left of the wind speed distribution and a decrease in the frequency of higher wind speeds.

3.14 Specific Humidity Projections

Figure 3.32a shows that annual specific humidity (the amount of water vapour in the atmosphere calculated as the ratio of the mass of water vapour to the total mass of the air parcel) is projected to increase substantially by the middle of the century for both the RCP4.5 (mean value 8%) and RCP8.5 (mean value 11%) scenarios. There exists a clear south-west to north-east gradient in the projections, with the largest increases in the north. For reference, the "observed" mean annual specific humidity (g kg^{-1}), as resolved by a high-resolution (1.5-km) downscaled ERA-Interim climate simulation, is presented in Figure 3.32b. Please refer to Flanagan *et al*. (2019) for an overview of the climate simulation configuration and validation results.

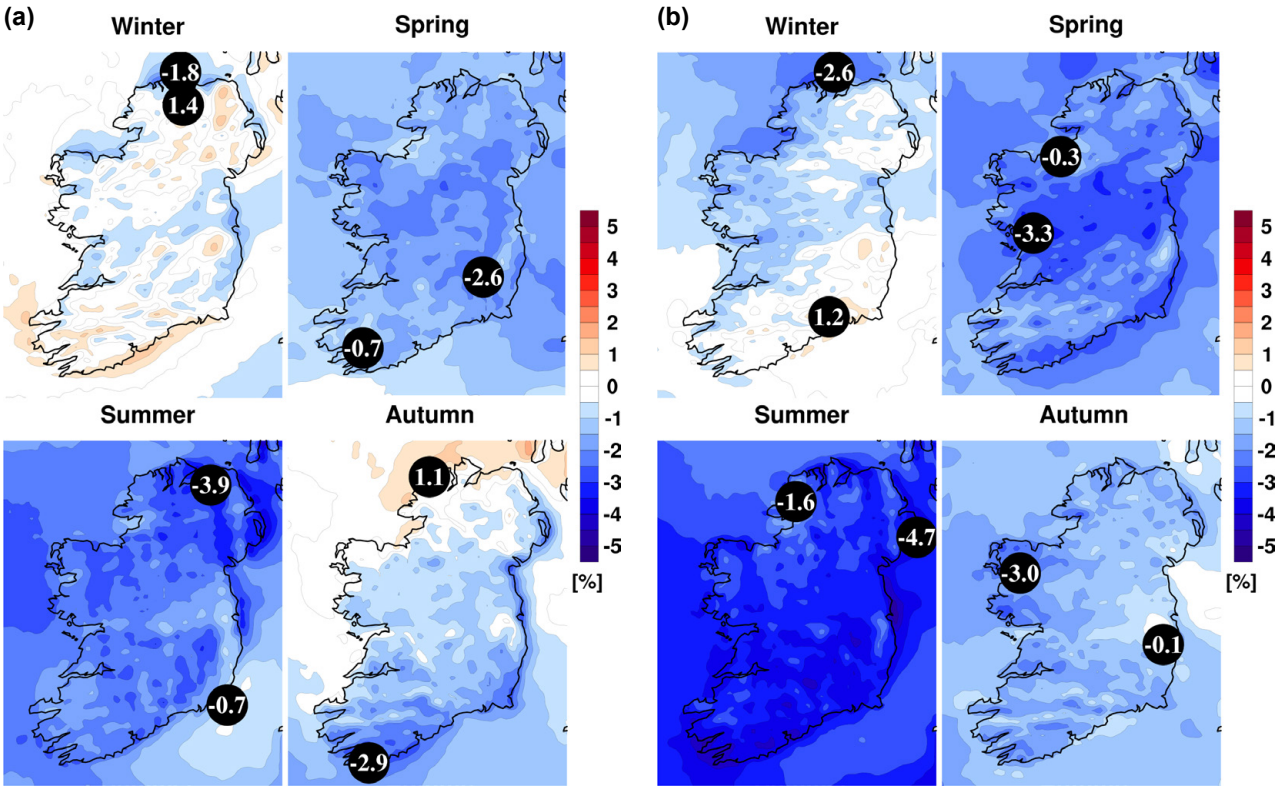

Figure 3.31. Seasonal projected change in the standard deviation of 10-m wind speed (%) for the (a) RCP4.5 and (b) RCP8.5 scenarios. In each case, the future period, 2041–2060, is compared with the past period, 1981–2000. The numbers included on each plot are the minimum and maximum projected changes, displayed at their locations.

Figure 3.33 presents the projected seasonal change (%) in specific humidity for the RCP4.5 and RCP8.5 scenarios. All seasons show a large expected increase in specific humidity. The increases are largest for autumn under the RCP8.5 scenario. Figure 3.34 shows a small variation between the 33rd, 50th and 66th projection percentiles for all seasons and both RCP scenarios. This result demonstrates

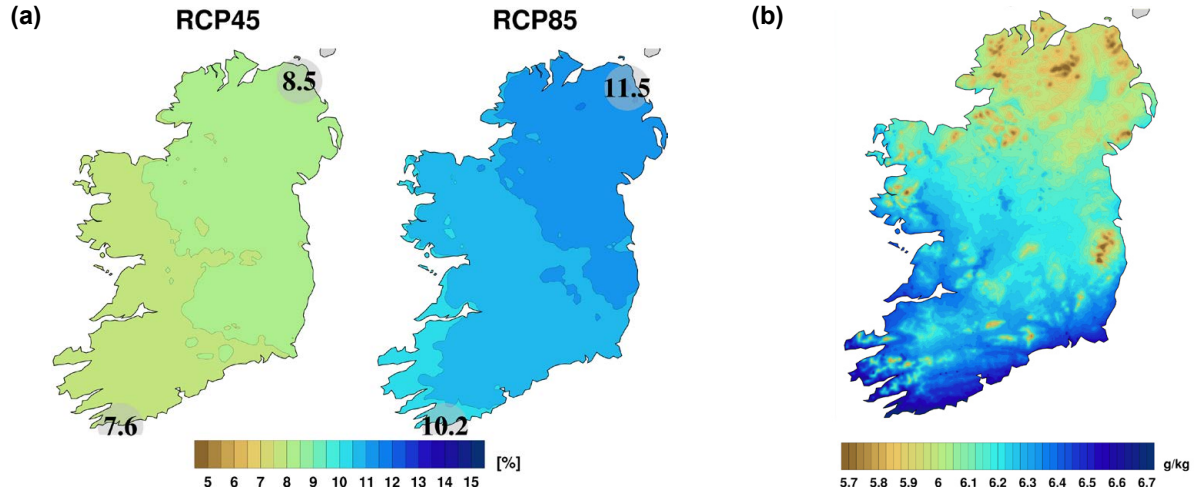

Figure 3.32. (a) Ensemble mean of mid-century specific humidity projections (%) for the RCP4.5 and RCP8.5 scenarios. In each case, the future period, 2041–2060, is compared with the past period, 1981–2000. The numbers included on each plot are the minimum and maximum projected changes, displayed at their locations. (b) Annual mean specific humidity (g kg^{-1}) as resolved by COSMO5-CLM-ERA-Interim 1.5-km data (1981–2000).

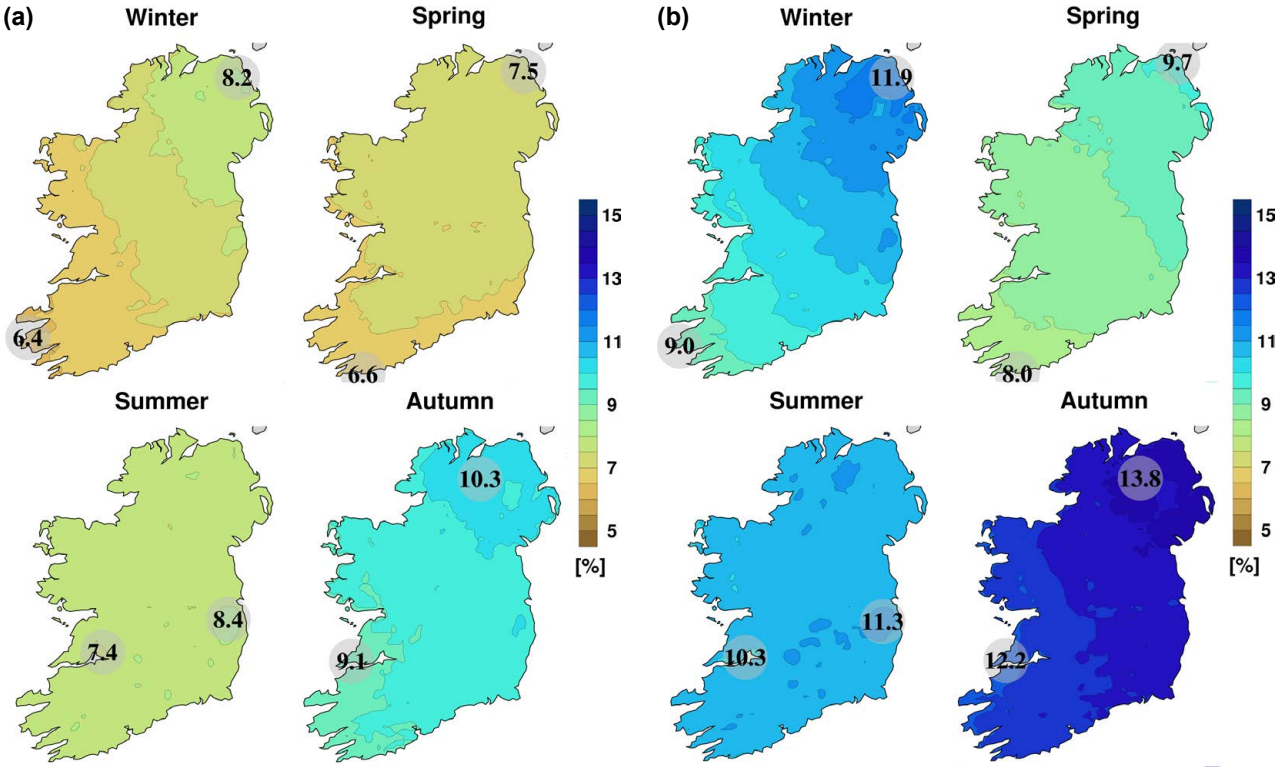

Figure 3.33. Mid-century seasonal projections of specific humidity (%) for the (a) RCP4.5 and (b) RCP8.5 scenarios. In each case, the future period, 2041–2060, is compared with the past period, 1981–2000. The numbers included on each plot are the minimum and maximum projected changes, displayed at their locations.

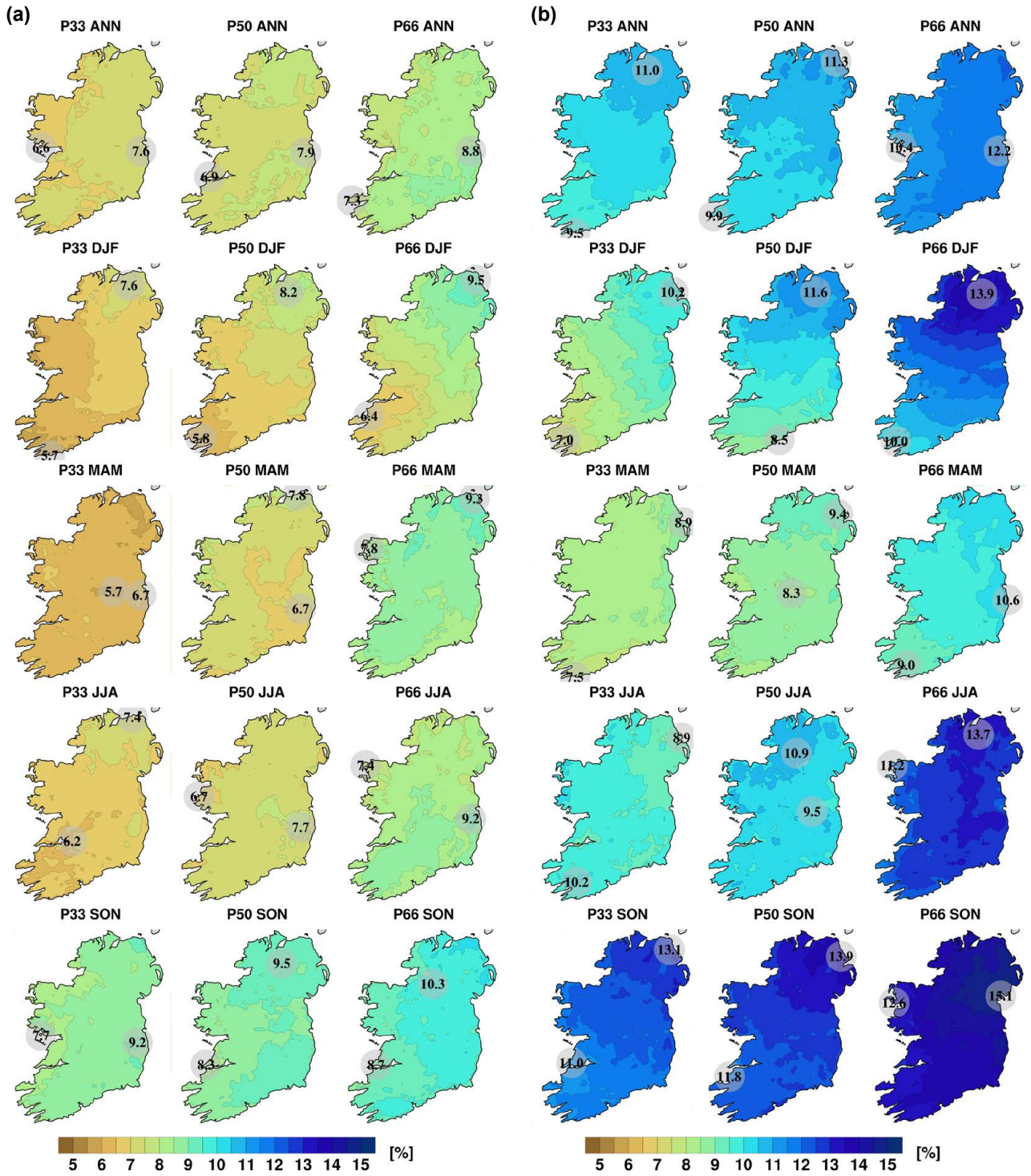

Figure 3.34. The 33rd, 50th and 66th percentiles of annual and seasonal mean specific humidity projections (%) for the (a) RCP4.5 and (b) RCP8.5 scenarios. In each case, the future period, 2041–2060, is compared with the past period, 1981–2000. The numbers included on each plot are the minimum and maximum projected changes, displayed at their locations. ANN, annual; DJF, December, January, February; JJA, June, July, August; MAM, March, April, May; SON, September, October, November.

good agreement (small spread) between ensemble members and adds a high level of confidence to the projections. Averaged over the whole country, the "likely" projected increases in mid-century specific humidity are 7% (annual RCP4.5), 10% (annual RCP8.5), 7% (winter RCP4.5), 9% (winter RCP8.5), 6% (spring RCP4.5), 8% (spring RCP8.5), 7%

(summer RCP4.5), 10% (summer RCP8.5), 9% (autumn RCP4.5) and 12% (autumn RCP8.5).

Specific humidity has direct impacts on animal and human health. Epidemiological studies indicate that low levels of specific humidity are associated with greater influenza mortality (e.g. Shaman *et al*., 2010, 2011; Tamerius *et al*., 2013). Barreca and Shimshack (2012) showed that the humidity–influenza relation is nonlinear, with lower specific humidity levels resulting "in greater influenza mortality at mean daily specific humidity levels below 6 g kg^{-1}", and that "incremental changes in humidity do not significantly affect influenza mortality when mean daily specific humidity exceeds a 6 g kg^{-1} threshold". An increase in specific humidity will amplify the adverse effects of increases in extreme temperatures (section 3.2) and heatwaves (section 3.3) and lead to higher mortality by limiting heat loss through evaporative cooling (Coffel *et al*., 2017).

3.15 Relative Humidity Projections

Relative humidity is the ratio of the amount of water vapour present in the air to the greatest amount possible at the same temperature. Warm air can hold substantially more moisture than cold air, meaning that the relative humidity of cold air is far higher than that of warm air for equal absolute humidity levels. Relative humidity is expressed as a percentage, with 0% corresponding to totally dry air and 100% to totally saturated air (leading to increased probability of precipitation).

Figure 3.35a presents the mean annual change (%)[12] in surface relative humidity for the RCP4.5 and RCP8.5 scenarios. The projections show a slight increase in relative humidity of ≈0–0.6% (mean value 0.1%) for the RCP4.5 scenario and 0–1% (mean value 0.35%) for the RCP8.5 scenario. There exists a south-east to north-west gradient in the projections, with the largest increases in the north. For reference, "observed" mean annual relative humidity (%), as resolved by a high-resolution (1.5-km) downscaled ERA-Interim climate simulation, is presented in Figure 3.35b. Please refer to Flanagan *et al*. (2019) for an overview of model configuration and validation.

Figure 3.36 presents the seasonal change (%) in relative humidity for the RCP4.5 and RCP8.5 scenarios. All seasons, with the exception of summer, show an increase (or ≈0% change) in relative humidity. The largest increases are noted for spring (both RCP scenarios) and winter (RCP8.5). For summer, relative humidity is projected to decrease in the south-east and increase in the north-west (both RCP scenarios).

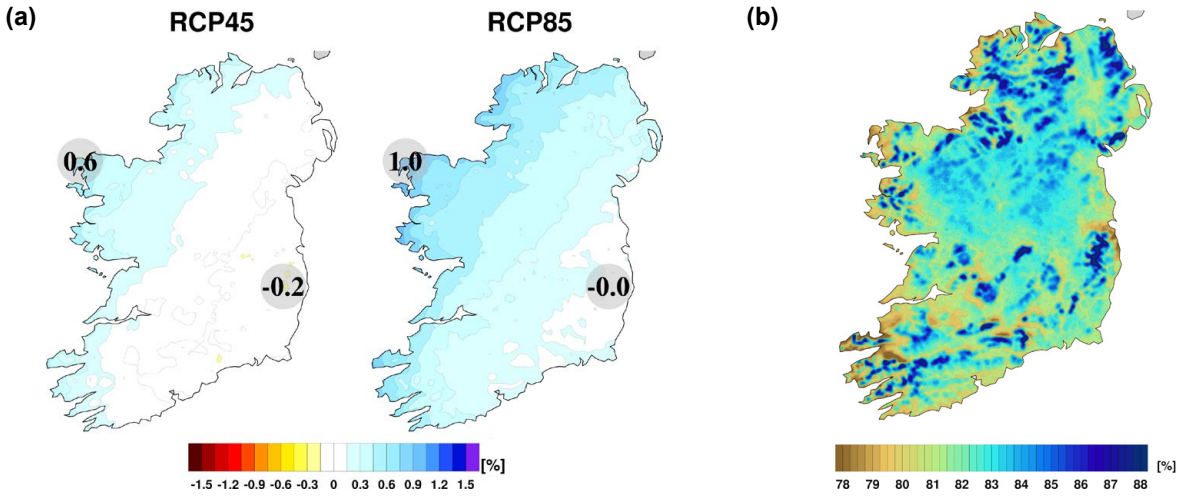

Figure 3.35. (a) Ensemble mean of mid-century relative humidity projections (%) for the RCP4.5 and RCP8.5 scenarios. In each case, the future period, 2041–2060, is compared with the past period, 1981–2000. The numbers included on each plot are the minimum and maximum projected changes, displayed at their locations. (b) Annual mean relative humidity (%) as resolved by COSMO5-CLM-ERA-Interim 1.5-km data (1981–2000).

12 For relative humidity, rather than a relative percentage change, climate projections (%) are calculated as "future (%) minus past (%)".

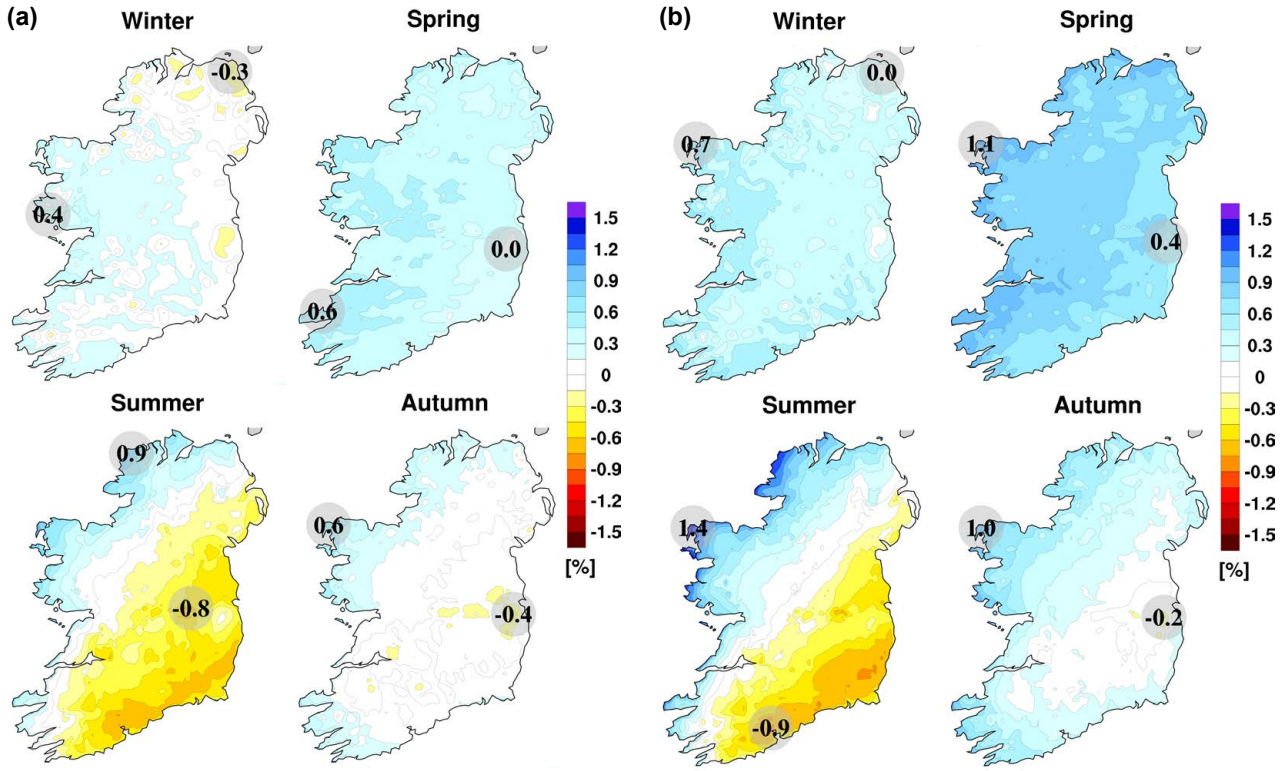

Figure 3.36. Mid-century seasonal projections of relative humidity (%) for the (a) RCP4.5 and (b) RCP8.5 scenarios. In each case, the future period, 2041–2060, is compared with the past period, 1981–2000. The numbers included on each plot are the minimum and maximum projected changes, displayed at their locations.

The percentile projection figures, presented in Figure 3.37, show a small variation between the 33rd, 50th and 66th for winter (RCP8.5), spring (both scenarios), over the full year (RCP8.5) and, to a lesser extent, during autumn (RCP8.5). The signal of decreases in the south-east and increases in the north-west during summer is evident for all percentiles and both RCPs. This agreement adds a level of confidence to the projected changes for summer (both RCPs) and the projected increases for spring (both RCPs), winter (RCP8.5), autumn (RCP8.5) and annual (RCP8.5).

The projections are somewhat contrary to the general consensus in the scientific literature that relative humidity will decrease over land in a warming climate. For example, Byrne and O'Gorman (2018) showed that in recent decades (1979–2016) the land surface has warmed substantially more than the ocean surface and, consequently, relative humidity has fallen over land. Declining relative humidity over land is also the dominant feature of future climate projections, with models predicting that future changes in surface temperature will be strongly amplified over land (Sutton *et al*., 2007; Byrne and O'Gorman, 2013) and that relative humidity will decline over land and either increase (M. Collins *et al*., 2013) or remain approximately constant (O'Gorman and Muller, 2010; Byrne and O'Gorman, 2016) over the oceans. However, the projected trend of decreasing relative humidity over land is not universal. For example, the CMIP5 ensemble of global projections show a projected increase in relative humidity in some coastal land regions, such as West Africa, the Middle East and India (e.g. Figure 1a of Byrne *et al*., 2016; Figure 12.21 of M. Collins *et al*., 2013). The projections over Ireland are small and a large projected increase is noted over the North Atlantic region directly to the north and west of Ireland (which is particularly noticeable in Figure 1a of Byrne *et al*., 2016). Sloth *et al*. (2012) analysed the ENSEMBLES dataset, a large ensemble of RCM climate projections for Europe (van der Linden *et al*., 2009), and found a mixed signal for mid-century projections of relative humidity, with a number of ensemble members showing an increase in relative humidity, particularly over Ireland and Northern Europe